

Safety-Aware Reinforcement Learning for Control via Risk-Sensitive Action-Value Iteration and Quantile Regression

Clinton Enwerem, Aniruddh G. Puranic, John S. Baras, and Calin Belta

Institute for Systems Research

University of Maryland, College Park, United States

{enwerem, puranic, baras, calin}@umd.edu

Abstract: Mainstream approximate action-value iteration reinforcement learning (RL) algorithms suffer from overestimation bias, leading to suboptimal policies in high-variance stochastic environments. Quantile-based action-value iteration methods reduce this bias by learning a distribution of the expected cost-to-go using quantile regression. However, ensuring that the learned policy satisfies safety constraints remains a challenge when these constraints are not explicitly integrated into the RL framework. Existing methods often require complex neural architectures or manual tradeoffs due to combined cost functions. To address this, we propose a risk-regularized quantile-based algorithm integrating Conditional Value-at-Risk (CVaR) to enforce safety without complex architectures. We also provide theoretical guarantees on the contraction properties of the risk-sensitive distributional Bellman operator in Wasserstein space, ensuring convergence to a unique cost distribution. Simulations of a mobile robot in a dynamic reach-avoid task show that our approach leads to more goal successes, fewer collisions, and better safety-performance trade-offs compared to risk-neutral methods.

Keywords: Distributional reinforcement learning, action-value iteration, quantile regression, risk-sensitive decision-making, safety-critical control.

1 Introduction

Standard Reinforcement Learning (RL) methods optimize expected cumulative cost but often use *misaligned* or *underspecified* cost functions that oversimplify real-world safety constraints, leading to overlooked risks. This limitation hinders deployment in high-risk domains where safety is crucial [1]. For instance, a risk-neutral autonomous robot may reach deadlock states, jeopardizing its mission and causing severe consequences [2]. Addressing this requires integrating explicit safety constraints to prevent risky behavior while preserving essential exploration.

Approximate Action-Value Iteration (hereafter, AVI) methods [3, 4, 5] estimate the action-value function using a neural network trained on the temporal difference between a current estimate of the action value and an observed *target* value (i.e., the sum of the stage cost and the expected future action value). However, in high-variance environments, these methods often suffer from overestimation bias, where the action-value approximation predicts values that are significantly higher than the true values [6]. AVI methods based on quantile regression [6, 7] address this by learning a quantile distribution of Q-values instead of a single expected value, reducing overestimation and improving estimation accuracy. By updating value distributions across quantile fractions, quantile regression RL algorithms enhance exploration and stabilize policy learning [6].

While distributional RL mitigates overestimation bias, it struggles with instantaneous stage cost misspecification, leading to unsafe or suboptimal policies [1]. Modifying stage costs to encode safety constraints [8, 9] is common but challenging to tune, especially in environments with varied risks [10] (Fig. 1). Safe Policy Optimization [11] addresses this by enforcing safety by training a

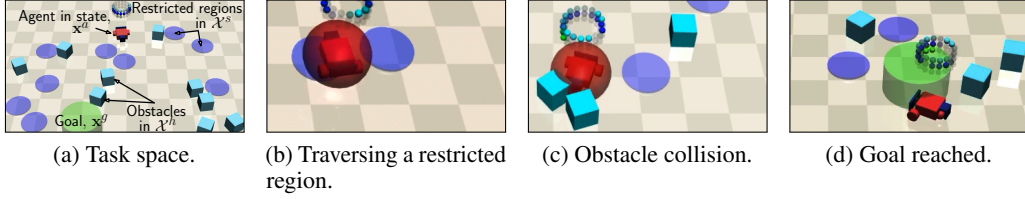


Figure 1: **Reach-avoid navigation task:** Close-ups from our experiments (Section 6) showing a differentially-driven mobile robot (depicted by a red car-like object in (a) and (d)) that is tasked with navigating to a uniformly randomized 2D goal location (green cylinder), denoted by $\mathbf{x}^g = [x^g, y^g]^\top$, with $x^g, y^g \in [-1, 1]$. En route to the goal, the robot must also avoid two regions within its environment: a traversable region, denoted by \mathcal{X}^s comprising purple discs shown in (b) (acting as a *soft* constraint), as well as obstacles (represented by light blue cubes in (c)) that inhibit the robot’s motion upon collision (i.e., a *hard* constraint). These static hazards and obstacles incur *distinct* costs that the agent must minimize while learning to safely navigate to the goal.

separate network, which is computationally expensive [12]. Furthermore, in dynamic environments, uncertainty from stochastic transitions, noise, perturbations, and model approximations can lead to brittle policies if not properly addressed [13]. To balance instantaneous stage cost optimization, safety adherence, and uncertainty mitigation – without the overhead of a separate cost network [11, 12] – we propose an RL framework that integrates risk-sensitive decision-making into approximate action-value iteration algorithms. This is achieved by augmenting the quantile loss with a risk term derived from experience-based cost distributions, to penalize safety violations.

Contributions and Paper Outline

- i. *Risk-regularized Quantile-Regression Based Approximate Action-Value Iteration (QR-AVI)* (Section 4): We enhance efficiency and safety by training a single quantile-based action-value iteration using a risk-regularized loss that integrates quantile regression with a penalty for safety violations (Section 4.3).
- ii. *Empirical uncertainty quantification via Kernel Density Estimation* (Sections 2.4 and 4.1): We approximate the cost distribution using Kernel Density Estimation (KDE), providing a probabilistic measure of safety constraints based on cost samples and enabling risk computation.
- iii. *Contraction & Finite-Time Convergence Guarantees* (Section 5): We prove the contraction of the risk-regularized Bellman operator, ensuring stable learning and finite-time convergence of the quantile-based action-value iteration to a stationary policy, leveraging the convexity of the quantile and risk loss terms.
- iv. *Modular RL Algorithmic Framework* (Section 4): We introduce a risk-sensitive QR-AVI algorithm (Algorithm 1) within a flexible, modular framework that integrates safety constraints into the quantile loss, making our approach applicable to other approximate RL methods.
- v. *Reach-Avoid Experiments (Section 6) & Comparative Study (Section 6.2)*: We evaluate a simulated car-like agent in a dynamic reach-avoid task, comparing our algorithm to nominal and risk-neutral variants. Results show improved safety, reduced quantile loss, and higher success rates.

2 Background

2.1 Reinforcement Learning (RL)

The terminology in this subsection follow [14]. We consider an *agent* is a decision-making entity that learns from interacting with an external *environment* through a sequence of *observations* (of its states and those of the environment), *actions*, and *costs*. At each discrete time step $t \in \mathbb{Z}_+$, the agent observes its current state as well as the current state of the environment, denoted for simplicity by the vector $\mathbf{x}_t = [\mathbf{x}_t^a, \mathbf{x}_t^e]^\top \in \mathcal{X} = \mathcal{X}_a \times \mathcal{X}_e$, where $\mathbf{x}_t^a \in \mathcal{X}_a$ represents the agent’s state, and $\mathbf{x}_t^e \in \mathcal{X}_e$

represents the environment's state, i.e., every artifact within the environment outside the agent. The agent applies a control input $\mathbf{u}_t \sim \mu(\cdot | \mathbf{x}_t^a) \in \mathcal{U}$ according to a (randomized) policy or control law $\mu : \mathcal{X}_a \rightarrow \Delta(\mathcal{U})$, where \mathcal{U} denotes the control space representing the discrete set of permissible control inputs, $\Delta(\mathcal{U})$ is the set of distributions over the control space, and where we require that $\sum_{\mathbf{u}_t \in \mathcal{U}} \mu(\mathbf{u}_t | \mathbf{x}_t^a) = 1, \forall \mathbf{x}_t^a \in \mathcal{X}_a$. The agent also incurs a cost $g_t \in \mathbb{R}$, defined by $g_t = \phi(\mathbf{x}_t^a, \mathbf{u}_t)$, based on its state and chosen control, and transitions to a new state $\mathbf{x}_{t+1}^a = f^a(\mathbf{x}_t^a, \mathbf{u}_t)$, where f^a is the state transition function that governs how the agent's states evolve over time. The environment does not make any decisions but transitions according to the random state transition law, $\mathbf{x}_{t+1}^e \sim f^e(\mathbf{x}_t^e)$. We define the system in which the agent interacts with the environment by a Markov Decision Process (MDP), which is given mathematically as the tuple $\mathcal{M} = (\mathcal{X}, \mathcal{U}, f^a, f^e, \phi, \gamma)$, where the arguments are as described hitherto, and γ is a discount factor for expected future costs.

Example 1. Consider the mobile navigation environment shown in Fig. 1, where the robot's dynamics are described in Section 6. The state space of the robot \mathcal{X}_a is comprised of the following information: wheel orientation, angular velocity, linear velocity, acceleration, magnetic flux, lidar measurements for the goal and obstacles, and Boolean indicators for the robot colliding with obstacles. The set of control inputs \mathcal{U} is 2-dimensional and consists of the torques applied to the left and right wheels. The stage cost $g_t \in \mathbb{R}$ is a function of the Euclidean distance between the robot and goal location at each timestep (see Section 6).

2.2 Action-Value Iteration (AVI)

In an MDP, the agent seeks a policy μ that minimizes the expected cumulative cost. The optimal cost-to-go function satisfies $J^*(\mathbf{x}) = \min_{\mathbf{u}_t} Q^*(\mathbf{x}_t, \mathbf{u}_t)$, where $Q^*(\mathbf{x}_t, \mathbf{u}_t)$ is the optimal action-value function. The action-value function $Q(\mathbf{x}_t, \mathbf{u}_t)$, which estimates the future cost from a given state-action pair, is updated iteratively using the Bellman recursion:

$$Q(\mathbf{x}_t, \mathbf{u}_t) \leftarrow Q(\mathbf{x}_t, \mathbf{u}_t) + \alpha^t [\phi(\mathbf{x}_t, \mathbf{u}_t) + \gamma \min_{\mathbf{u}_{t+1}} Q(\mathbf{x}_{t+1}, \mathbf{u}_{t+1}) - Q(\mathbf{x}_t, \mathbf{u}_t)], \quad (1)$$

where $\phi(\mathbf{x}_t, \mathbf{u}_t)$ is the stage cost, $\alpha^t \in (0, 1]$ is the learning rate, and $\gamma \in (0, 1]$ is a discount factor. However, maintaining exact action values for all state-control pairs is impractical in large state-control spaces, necessitating approximation.

2.3 Approximate AVI via Quantile Regression

Approximate action-value iteration methods replace the tabular representation with a function approximator, such as a θ -parameterized neural network, i.e., $Q(\mathbf{x}_t, \mathbf{u}_t) \approx Q(\mathbf{x}_t, \mathbf{u}_t; \theta)$, that is typically trained using data sampled uniformly from a sequence of state-control pairs, \mathcal{D} , containing tuples of the form $\{(\mathbf{x}_t, \mathbf{u}_t, g_t, \mathbf{x}_{t+1}, d_t)\}$, where d_t is a Boolean indicator variable that signifies if a learning episode has ended. The predicted Q-values (denoted by $Q(\mathbf{x}_t, \mathbf{u}_t; \theta)$) are updated by minimizing the loss function defined by

$$\mathcal{L}(\theta_i) = \mathbb{E}[(y_i - Q(\mathbf{x}_t, \mathbf{u}_t; \theta_i))^2], \quad i = 1, 2, \dots, B, \quad (2)$$

where B is the size of the batch sampled from \mathcal{D} , y_i is the i^{th} target action-value realized from a target network, $Q(\mathbf{x}_t, \mathbf{u}_t; \theta_i)$, with parameters, θ_i that are updated with a predetermined frequency to converge at a stable or low-variance value: $y_i := g_t + \gamma \min_{\mathbf{u}_{t+1}} Q(\mathbf{x}_{t+1}, \mathbf{u}_{t+1}; \theta_i)$. To account for variability in the Q-value distribution, quantile regression-based approximate AVI (QR-AVI) methods [6, 7] estimate the target action-value distribution using a set of quantiles. Specifically, in the QR-AVI framework [7], the loss in (2) is replaced by the quantile regression loss (or Huber quantile loss) given by the following equation:

$$\mathcal{L}_{\text{QR}}(\hat{\theta}) = \frac{1}{N_\tau} \sum_{n=1}^{N_\tau} \mathbb{E} \left[\rho_{\tau_n}^\kappa \left(y_j - \hat{\theta}_n(\mathbf{x}_t, \mathbf{u}_t) \right) \right]. \quad (3)$$

In (3), $y_j = g_t + \gamma \hat{\theta}_j(\mathbf{x}_{t+1}, \mathbf{u}_{t+1})$ defines the j^{th} quantile (of the target action-value distribution) that depends on the system's (agent-environment) transition dynamics and stage cost, with $j \in$

$\{1, \dots, N_\tau\}$, N_τ is the prescribed number of quantile fractions, and $\rho_{\tau_n}^\kappa$ is the asymmetric Huber loss (with parameter κ) corresponding to the uniformly-distributed quantile fraction, $\tau_n \in (0, 1)$ (δ_w is the Dirac delta function at $w \in \mathbb{R}$ and $n = 1, 2, \dots, N_\tau$):

$$\rho_{\tau_n}^\kappa(m) = |\tau_n - \delta_{\{m < 0\}}| \mathcal{L}_\kappa(m), \quad \tau_n = (n-0.5)/N_\tau \quad (4)$$

$$\mathcal{L}_\kappa(m) = \begin{cases} \frac{1}{2}m^2, & \text{if } |m| \leq \kappa, \\ \kappa(|m| - \frac{1}{2}\kappa), & \text{otherwise.} \end{cases} \quad (5)$$

Remark 1 (Parameters of \mathcal{L}_{QR}). : In (3), $\hat{\theta}_j(\mathbf{x}_{t+1}, \mathbf{u}_{t+1})$ is the estimated future action-value distribution for the next state-control pair $(\mathbf{x}_{t+1}, \mathbf{u}_{t+1})$, corresponding to the j -th quantile fraction. This term reflects the predicted distribution of future costs under the current policy. The Huber loss function, $\rho_{\tau_n}^\kappa(m)$ is a loss function that minimizes the action-value distribution approximation error for the n -th quantile by combining the squared error and absolute error and switching between these errors based on a threshold parameter κ , a strategy that makes the Huber loss robust to outliers [7], which is important for real-world control applications with noisy or uncertain data. The Dirac function adjusts the magnitude of the error based on the sign of the desired cost-to-go, m , to differentiate between underestimation and overestimation of the action value distribution.

2.4 Data-Driven Uncertainty Quantification

Since the agent can choose from multiple possible actions $\mathbf{u}_t \in \mathcal{U}$ at each state \mathbf{x}_t^a , each action incurs a stage cost, given by $\phi(\mathbf{x}_t^a, \mathbf{u}_t)$, but it may also violate safety constraints that are not captured by the stage cost function (see Example 1 and Fig. 1a). These safety violations contribute to additional costs (hereafter *violation costs*), which we model *separately* as the non-negative random variable, C_t . We assume C_t follows an unknown distribution with probability density, P_c , that must be learned from cost samples in the sampled batch, $\{C_t^{(1)}, C_t^{(2)}, \dots, C_t^{(|B|)}\}$, for each time step, where $C_t^{(e)}$ is the violation cost incurred at time step t in episode e . Thus, the cost distribution at a state \mathbf{x}_t is conditioned on μ .

Definition 1 (Policy-Conditioned Cost Distribution). Given a policy, μ , and a cost distribution, P_c , the policy-conditioned cost distribution at state \mathbf{x}_t (hereafter denoted by $Z_c^\mu(\cdot | \mathbf{x}_t^a)$) is the cost distribution obtained by marginalizing over inputs realized from μ , given by:

$$\sum_{\mathbf{u}_t \in \mathcal{U}} \mu(\mathbf{u}_t | \mathbf{x}_t^a) P_c(\cdot | \mathbf{x}_t^a, \mathbf{u}_t), \quad (6)$$

where $P_c(\cdot | \mathbf{x}_t^a, \mathbf{u}_t)$ is a distribution of safety violation costs associated with the state control pair, $(\mathbf{x}_t^a, \mathbf{u}_t)$. For instance, if C_t is the cost incurred from violating a safety constraint, $P_c(C_t | \mathbf{x}_t^a, \mathbf{u}_t)$ provides the likelihood of incurring a particular cost C_t given the pair, $(\mathbf{x}_t^a, \mathbf{u}_t)$.

Remark 2 (Challenges with Computing $Z_c^\mu(\cdot | \mathbf{x}_t^a)$). Equation (6) provides a formal framework that fully captures the cost distribution for a given state and under control inputs chosen according to a policy. Unfortunately, due to the unavailability of an exact form of $P_c(\cdot | \mathbf{x}_t^a, \mathbf{u}_t)$, a direct computation of a closed form expression for $Z_c^\mu(\cdot | \mathbf{x}_t^a)$ becomes infeasible. This challenge thus necessitates the need for an approximation of $Z_c^\mu(\cdot | \mathbf{x}_t^a)$, hereafter denoted as \hat{Z}_c^μ , from costs sampled from stored experience during training.

2.5 Risk Model

Definition 2 (Risk Measure). Consider the probability space, $(\Omega, \mathcal{F}, \hat{Z}_c^\mu)$, where $\Omega \supseteq \mathcal{X} \times \mathcal{U}$ is the sample space and \mathcal{F} is the σ -algebra over Ω . Suppose \mathcal{C} denotes the set of all cost random variables defined on Ω . Omitting the time argument for brevity, we define the risk measure as a function $\hat{\rho}_\beta : \mathcal{C} \rightarrow \mathbb{R}$ that assigns a real number representing the risk or variability of C , i.e., $\hat{\rho}_\beta$ captures the tail behavior of the cost distribution; $\beta \in (0, 1)$ is the confidence level representing the proportion of \hat{Z}_c^μ that is covered when computing $\hat{\rho}_\beta$.

Hereafter, we focus on *coherent* risk measures, widely used in risk-sensitive optimization, that satisfy key axioms: sub-additivity, positive homogeneity, translation invariance, monotonicity, and risk-utility duality [15, 16, 17]. Of these, we select the Conditional Value-at-Risk (CVaR), since it can distinguish between tail events [15] beyond β .

2.6 Risk Measure Computation

Given the cost distribution \hat{Z}_c^μ realized from some estimation scheme (see Section 4.1), the expected cost at time step t can be computed as:

$$\mathbb{E}[C_t] = \frac{1}{B} \sum_{e=1}^B C_t^{(e)}. \quad (7)$$

Using (7), and specializing our discussion to the β -level CVaR (denoted as CVaR_β) is given by

$$\text{CVaR}_\beta(C_t) = \mathbb{E}[C_t \mid C_t \geq \text{VaR}_\beta(C_t)], \text{ where} \quad (8)$$

$$\text{VaR}_\beta(C_t) = \inf_{\star} \{\star \in \mathbb{R} \mid \hat{Z}_c^\mu(C_t \leq \star) \geq \beta\} \quad (9)$$

is the Value-at-Risk or β^{th} percentile of \hat{Z}_c^μ .

3 Problem Formulation

Assume the setting in Section 2.1. Given an MDP representing the system, we wish to find a policy that minimizes the expected cumulative cost while minimizing the risk of safety constraint violations, that is, the *risk-sensitive* cumulative cost, where the risk is computed from an estimated (constraint-violation) cost distribution. Formally, we consider the following problem:

Problem 1. *Given an MDP (Section 2.1), a stage cost function, ϕ , a cost distribution, \hat{Z}_c^μ , and an initial state, \mathbf{x}_0 , find a policy μ^* such that:*

$$\mu^* = \arg \min_{\mu} \mathbb{E} \left[\sum_{t=0}^{T-1} \alpha^t \phi(\mathbf{x}_t, \mathbf{u}_t) \right] + \lambda [\hat{\rho}_\beta \left(\sum_{t=0}^{T-1} C_t \right)]. \quad (10)$$

In (10), $\hat{\rho}_\beta$ denotes the β -level CVaR corresponding to \hat{Z}_c^μ , estimated from cost samples collected during each episode, λ is a positive scalar regularization parameter that balances the cumulative stage cost minimization and risk minimization, and $C_t \sim \hat{Z}_c^\mu$ is the violation cost random variable. To solve Problem 1, we propose a risk-sensitive QR-AVI algorithm, with the risk computation enabled by Kernel Density Estimation (KDE). In Section 6.3.3, we provide a more application-centered argument in support of our choice of KDE, while Section 4 (appearing next) describes the specifics of our approach that draw on recent advances in risk-sensitive RL [13, 18, 19, 20, 21, 22].

4 Approach: Risk-Regularized Quantile-Based AVI with KDE-Based Cost Distribution Estimation

4.1 KDE-Based Estimation of Z_c^μ

Following the discussions in Section 2.4 and for reasons outlined in Remark 2, we employ Kernel Density Estimation (KDE) [23], a technique that provides a practical method to approximate the policy-conditioned cost distribution (see Definition 1) from finite training samples. By leveraging observed costs during policy execution, KDE constructs an empirical distribution, \hat{Z}_c^μ (11), as a proxy for Z_c^μ , that enables the computation of distributional statistics essential for risk-sensitive decision-making. Denoting the cost samples observed from the training data at time step t by $\mathcal{C}_t := \{C_t^{(i)}\}_{i=1}^B$, we can write the likelihood of C_t as:

$$\hat{Z}_c^\mu(C_t \mid \mathbf{x}_t) = \frac{1}{Bh} \sum_{i=1}^B k \left(\frac{C_t - C_t^{(i)}}{h} \right), \quad C_t^{(i)} \in \mathcal{C}_t, \quad (11)$$

where k is the kernel function, and $h > 0$ is the bandwidth.

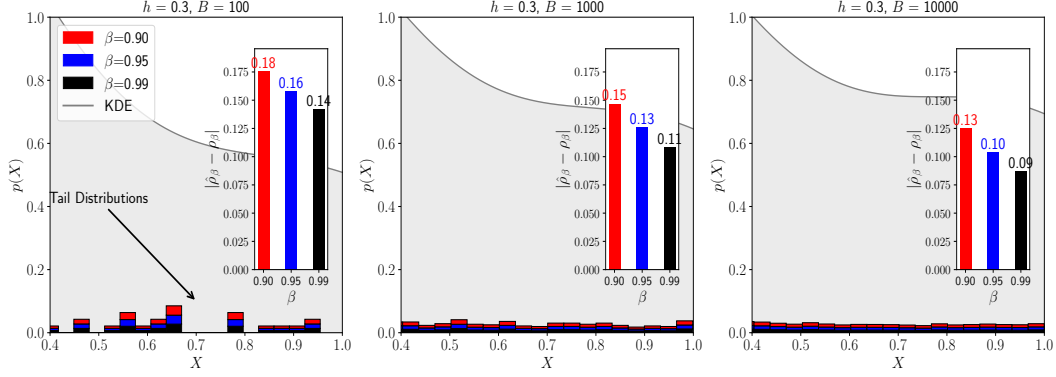


Figure 2: Graphing the KDE-estimated probability density ($p(X)$), shown as a gray line enclosing the gray-filled area) corresponding to samples of an uncertain variable (X). The inset bar plots show the evolution of the absolute error, $|\hat{\rho}_\beta - \rho_\beta|$, between the CVaR computed from $p(X)$ (i.e., $\hat{\rho}_\beta$) and the true CVaR (ρ_β) for an increasing number of KDE samples, $B = \{100, 1000, 10000\}$ and using a Gaussian kernel with a fixed bandwidth (h) of 0.3. The underlying data are from a heavy tailed distribution on $(0, 1]$. Notice how the CVaR estimate improves with the number of cost samples.

Remark 3 (Caveats on using KDE). While KDE approximates Z_c^μ by smoothing over observed cost values, thus capturing both aleatoric uncertainty (due to the inherent stochasticity in the costs) and epistemic uncertainty (due to finite cost samples) as opined in [24], its estimation accuracy improves with the number of samples [25]. However, limited experiments with a heavy-tailed distribution (see Fig. 2) suggest that higher values of B may not necessarily lead to substantial improvements in the accuracy of the distribution estimation.

4.2 Quantile Regression with Risk-Sensitive Loss Functions

As noted in Section 1, encoding safety with a monolithic cost function has limitations. To better capture safety risks, we propose the following risk-regularized loss function (\mathcal{L}) for QR-AVI (with $\lambda \in (0, 1)$):

$$\mathcal{L}(\theta) = (1 - \lambda)\mathcal{L}_{QR}(\theta) + \lambda\mathcal{L}_\rho(\hat{\rho}_\beta(C), c_{\max}), \quad (12)$$

where $\mathcal{L}_{QR}(\cdot)$ is the quantile regression loss given by (3), $\mathcal{L}_\rho(\cdot)$ is the loss corresponding to the risk (i.e., $\hat{\rho}_\beta(C)$; see (8)) computed over the cost distribution in (11), and c_{\max} is a positive cost threshold. By applying KDE on the observed cost samples \mathcal{C} , we can compute $\hat{\rho}_\beta(C)$ with respect to \hat{Z}_c^μ .

4.3 Risk-Sensitive Approximate Value Iteration with Learned Constraint-Violation Cost Distribution

With the KDE-estimated cost distribution, we construct the risk-sensitive loss function in (12) and train a function approximator that approximates the distribution of action-values using quantile regression. In the cost-minimizing context, two scenarios result from incorporating risk sensitivity in AVI, depending on β 's value: β values on $[0.9, 1)$ correspond to a *risk-averse* setting, while $\beta = 0.5$ corresponds to the *risk-neutral* setting, since the CVaR reduces to the expected value of the distribution [17].

Accordingly, to distinguish between these settings in our QR-AVI algorithm, each corresponding to a different instance of \mathcal{L} (see Table 1), we adopt the respective abbreviations: E-QR-AVI and ρ -QR-AVI. Our algorithm (Algorithm 1) trains a risk-sensitive function approximator for an action-value distribution by incorporating KDE-based risk estimation into the learning process. The key step that enables the computation of the risk loss is the storing of state-action-cost transitions in the replay buffer (Line 7 of Algorithm 1). To update the Q-network, we compute the risk loss using the KDE-estimated distribution of costs sampled from experience.

Algorithm 1: Risk-Sensitive Approximate Value Iteration	
Input: $T, \mathcal{D}, B, \gamma, \beta, \lambda, \kappa, \{\epsilon_t\}_{t=1}^T, \eta, N_\tau, c_{\max}$	
Output: Q_θ	
1	Initialize $Q_\theta, Q_{\theta'}, \mathcal{D}, \{\tau_n\}_{n=1}^{N_\tau}, d_t = \text{false}$
2	for $t = 1$ to T do
3	Observe state \mathbf{x}_t
4	while $d_t \neq \text{true}$ do // \mathbf{x}_{t+1} is not terminal
5	$\mathbf{u}_t \sim \epsilon_{t\text{-greedy}}$
6	Execute \mathbf{u}_t , compute g_t , observe $\mathcal{C}_t, \mathbf{x}_{t+1}, d_t$
7	Store $(\mathbf{x}_t, \mathbf{u}_t, g_t, \mathcal{C}_t, \mathbf{x}_{t+1}, d_t)$ in \mathcal{D}
8	if $ \mathcal{D} \geq B$ then
9	Sample batch B from \mathcal{D}
10	for
	$(\mathbf{x}_{t,j}, \mathbf{u}_{t,j}, g_{t,j}, \mathcal{C}_{t,j}, \mathbf{x}_{t+1,j}, d_{j,t})$
	in B do
11	$Q_{\text{target}} = g_{t,j} + \gamma(1 - d_{j,t}) \min_{\mathbf{u}_{t+1}} \mathbb{E}[\hat{\theta}(\mathbf{x}_{t+1,j}, \mathbf{u}_{t+1}, \tau)]$
12	UpdateNetwork $(Q_{\text{target}}, \mathcal{C}_{t,j}, \text{args}^*)$
	// Update target
13	$\theta' \leftarrow \eta\theta + (1 - \eta)\theta'$
14	$\mathbf{x} \leftarrow \mathbf{x}_{t+1}$

Table 1: Training Loss Functions ($C \sim \hat{Z}_c^\mu$)

Algorithm	Loss Function (\mathcal{L})
AVI	$(y - Q(\mathbf{x}, \mathbf{u}))^2$
QR-AVI	$\frac{1}{N_\tau} \sum_{n=1}^{N_\tau} \sum_{j=1}^{N_\tau} \overbrace{\rho_{\tau_n}^\kappa(y_j - \hat{\theta}_n)}^{\mathcal{L}_{\text{QR}}}$
\mathbb{E} -QR-AVI	$\underbrace{\lambda'}_{1-\lambda} \mathcal{L}_{\text{QR}} + \lambda[(\mathbb{E}[C] - c_{\max})^2]_+$
ρ -QR-AVI	$\lambda' \mathcal{L}_{\text{QR}} + \lambda[(\hat{\rho}_\beta(C) - c_{\max})^2]_+$

5 Theoretical Guarantees for Risk-Sensitive QR-AVI: Contraction, Fixed-Point Existence, & Finite-Time Convergence

Definition 3 (Risk-Sensitive Distributional Bellman Operator [26]). Let $Z \in \mathcal{Z}$ denote the expected cumulative cost distribution, with \mathcal{Z} given as $\mathcal{Z} = \{Z \mid \mathbb{E}[Z(\mathbf{x}, \mathbf{u})] < \infty, \forall \mathbf{x}, \mathbf{u}\}$. Let $\mathcal{Z}_c := \{Z_c^\mu \mid \mathbb{E}[Z_c^\mu(\mathbf{x}, \mathbf{u})] < \infty, \forall \mathbf{x}, \mathbf{u}\}$. Suppose $\hat{Z}_c^\mu \in \mathcal{Z}_c$ and $\hat{\rho}_\beta(\hat{Z}_c^\mu) \in \mathfrak{C} := \{C \mid C(\mathbf{x}^a) < \infty, \forall \mathbf{x}^a\}$, with $\hat{\rho}_\beta[\hat{Z}_c^\mu](\mathbf{x}^a) := \hat{\rho}_\beta(\hat{Z}_c^\mu[\cdot | \mathbf{x}^a])$. The risk-sensitive distributional Bellman operator, \mathcal{T}^β , corresponding to a β -level coherent risk measure, $\hat{\rho}_\beta$ (see Definition 2), is

$$\mathcal{T}^\beta Z(\mathbf{x}, \mathbf{u}) \stackrel{D}{=} g_t - \gamma \hat{\rho}_\beta[Z_c^\mu(\mathbf{x}_{t+1}, \mathbf{u}_{t+1})]. \quad (13)$$

$\stackrel{D}{=}$ denotes distributional equivalence, and $\mathbf{u}_{t+1} \sim \mu(\cdot | \mathbf{x}_{t+1})$.

Theorem 1 (Contraction of the Risk-Sensitive Bellman Operator with Cost-Based Risk Regularization). Assume the setting in Definition 3. Let Z_1 and Z_2 be two cumulative cost distributions, and suppose that $\hat{\rho}_\beta$ is non-expansive, i.e., that it satisfies the following relationship for two random costs, $C_1 \sim \hat{Z}_{1,c}^\mu$ and $C_2 \sim \hat{Z}_{2,c}^\mu$ (with $\hat{Z}_{1,c}^\mu \neq \hat{Z}_{2,c}^\mu$) $|\hat{\rho}_\beta(C_1) - \hat{\rho}_\beta(C_2)| \leq \|C_1 - C_2\|$. Let \hat{Z}_c^μ be related to Z by $\hat{Z}_c^\mu(\mathbf{u} | \mathbf{x}^a) = \Psi(Z(\mathbf{x}, \mathbf{u}))$, where $\Psi : \mathbb{R} \rightarrow \mathbb{R}_+$ is a coherent, Lipschitz continuous (with $L \leq 1$), and bounded function. Then, \mathcal{T}^β is a γ -contraction in the Wasserstein-1 (W_1) metric (see [7]), i.e., $W_1(\mathcal{T}^\beta Z_1, \mathcal{T}^\beta Z_2) \leq \gamma W_1(Z_1, Z_2)$.

Proof. Using (13), we can write:

$$\mathcal{T}^\beta Z(x, u) \stackrel{D}{=} \phi(\mathbf{x}, \mathbf{u}) - \gamma \hat{\rho}_\beta(Z_c^\mu(\mathbf{x}_{t+1}, \mathbf{u}_{t+1})), \quad (14)$$

so that by applying \mathcal{T}^β to Z_1 and Z_2 , we obtain:

$$\begin{aligned} \mathcal{T}^\beta Z_1 &= \phi(\mathbf{x}, \mathbf{u}) - \gamma \hat{\rho}_\beta(\hat{Z}_{1,c}^\mu), \\ \mathcal{T}^\beta Z_2 &= \phi(\mathbf{x}, \mathbf{u}) - \gamma \hat{\rho}_\beta(\hat{Z}_{2,c}^\mu). \end{aligned} \quad (15)$$

Taking W_1 , we obtain $W_1(\mathcal{T}^\beta Z_1, \mathcal{T}^\beta Z_2)$ as:

$$W_1(\phi(\mathbf{x}, \mathbf{u}) - \gamma \hat{\rho}_\beta(\hat{Z}_{1,c}^\mu), \phi(\mathbf{x}, \mathbf{u}) - \gamma \hat{\rho}_\beta(\hat{Z}_{2,c}^\mu)). \quad (16)$$

Since $\phi(\mathbf{x}, \mathbf{u})$ is deterministic, it cancels out, yielding

$$W_1(-\gamma \hat{\rho}_\beta(\hat{Z}_{1,c}^\mu), -\gamma \hat{\rho}_\beta(\hat{Z}_{2,c}^\mu)). \quad (17)$$

By the non-expansiveness of $\hat{\rho}_\beta$:

$$W_1(\hat{\rho}_\beta(\hat{Z}_{1,c}^\mu), \hat{\rho}_\beta(\hat{Z}_{2,c}^\mu)) \leq W_1(\hat{Z}_{1,c}^\mu, \hat{Z}_{2,c}^\mu). \quad (18)$$

Multiplying the L.H.S of (18) by γ , it follows that:

$$\begin{aligned} & W_1(-\gamma \hat{\rho}_\beta(\hat{Z}_{1,c}^\mu), -\gamma \hat{\rho}_\beta(\hat{Z}_{2,c}^\mu)) \\ &= \gamma W_1(\hat{\rho}_\beta(\hat{Z}_{1,c}^\mu), \hat{\rho}_\beta(\hat{Z}_{2,c}^\mu)) \leq \gamma W_1(\hat{Z}_{1,c}^\mu, \hat{Z}_{2,c}^\mu). \end{aligned} \quad (19)$$

By invoking the boundedness assumption on Z_c , we get:

$$W_1(\hat{Z}_{1,c}^\mu, \hat{Z}_{2,c}^\mu) \leq W_1(Z_1, Z_2). \quad (20)$$

By the assumptions on Ψ , there exists an L s.t.

$$W_1(\Psi(Z_1), \Psi(Z_2)) \leq L \cdot W_1(Z_1, Z_2). \quad (21)$$

Setting $\gamma = L$ and applying (13), we get:

$$W_1(\mathcal{T}^\beta Z_1, \mathcal{T}^\beta Z_2) \leq \gamma W_1(Z_1, Z_2). \quad (22)$$

Since $L \leq 1$ by assumption, it follows that \mathcal{T}^β is a contraction. \square

Corollary 1 (Existence of A Unique Cumulative Cost Distribution). *From Theorem 1, by Banach's fixed-point theorem [27], there exists a unique fixed point Z^* such that:*

$$Z^* = \mathcal{T}^\beta Z^*. \quad (23)$$

Proposition 1 (Finite-Time Convergence of the Risk-Sensitive QR-AVI Algorithm). *Suppose \mathcal{X} and \mathcal{U} are continuous and bounded, with \mathcal{L} and \mathcal{L}_ρ convex, and assume that the agent explores the environment sufficiently often¹. Then, under a fitting (diminishing) learning rate schedule, e.g.,*

$$\alpha^t = \frac{k_\alpha}{(t+1)}, \quad t = 0, 1, \dots, \quad (24)$$

where k_α is a positive constant that controls the rate of decay, the risk-sensitive algorithm will converge to a Pareto-optimal action-value in finite time.

Proof. Since both the quantile and risk-sensitive loss functions are convex, their combination is also convex for $\lambda \in (0, 1]$, guaranteeing a Pareto-optimal solution. The convexity ensures any local minimum is a global minimum, and sufficient exploration with an appropriate learning rate schedule ensures convergence to the unique Pareto-optimal action-value distribution in finite time. \square

6 Experiments

In this section, we provide a comprehensive overview of our experimental study, detailing our simulation setup, followed by our training and evaluation procedures, and concluding with comparisons with a risk-neutral variant.

¹Here, the exploration might be specified by an ϵ_t -greedy strategy, for instance, i.e., at time t , the agent in state \mathbf{x}_t takes a random action with probability $1 - \epsilon_t$.

6.1 Safety-Gymnasium Learning Environment

In this experiment, we aim to train a differentially-driven mobile robot (depicted as a red wheeled car in Fig. 1) to navigate to a randomized goal location ($\mathbf{x}_t^g \in \mathbb{R}_2$) while minimizing the cost of traversing restricted areas and avoiding obstacles. The robot is differentially-driven and equipped with a Lidar sensor to measure distances to various environmental features such as obstacles and the goal. The state space, control space, and the observations that the agent makes, as well as the goal of the experiment, are outlined below:

$$\mathcal{X} = \{\mathbf{x}_t = \mathbf{x}_t^a, \mathbf{x}_t^s, \mathbf{x}_t^h, \mathbf{x}_t^g \mid t = 1, 2, \dots, \}, \quad (25a)$$

$$\mathcal{U} = \{\mathbf{u}_t = [v_t^L, v_t^R] \mid t = 1, 2, \dots, \}, \quad (25b)$$

$$C_t(\mathbf{x}_t^a) = \begin{cases} c_t^s = c_s \sim \mathcal{U}_{[0,1]} \cdot \mathbb{I}_{\mathcal{X}^s}(\mathbf{x}_t^a) \\ c_t^h = c_h \sim \mathcal{U}_{[0,1]} \cdot \mathbb{I}_{\mathcal{X}^h}(\mathbf{x}_t^a), \end{cases} \quad (25c)$$

$$f^a(\mathbf{x}_t^a, \mathbf{u}_t) = \begin{cases} x_{t+1} &= x_t + \frac{r}{2} (v_t^R + v_t^L) \cos \theta_t, \\ y_{t+1} &= y_t + \frac{r}{2} (v_t^R + v_t^L) \sin \theta_t, \\ \theta_{t+1} &= \theta_t + \frac{r}{2d_w} (v_t^R - v_t^L). \end{cases} \quad (25d)$$

In (25), $\mathbf{x}_t^a = [x_t, y_t, \theta_t]^\top$ defines the robot's state vector comprising the position of its t -step center of curvature and orientation (θ_t). v_t^L and v_t^R are the robot's left and right wheel (linear) velocities, r is its wheel radius, d_w is the half-distance between the robot's two wheels, and $\mathbb{I}_{\mathcal{X}^*}$ is an indicator function. The environment contains 10 restricted region markers, 10 obstacles scattered around the map, and a single goal location. The location of the restricted regions, goal, and obstacle are randomized according to a uniform distribution, $\mathcal{U}_{(a,b)}$, with $a, b \in [-1, 1]$, *at the beginning of each episode and remain static till the episode ends*, i.e., after a prescribed number of time steps, T , have elapsed. In particular, after T time steps, $\mathbf{x}^e = [\mathbf{x}_t^s, \mathbf{x}_t^h, \mathbf{x}_t^g]^\top$ is:

$$\mathbf{x}_{t+T}^e = f^e(\mathbf{x}_t^e) := \mathbf{x}_t^e + \Delta \mathbf{x}_{t,t}^e, \Delta \mathbf{x}_{t,t}^e \sim \mathcal{U}_{(a,b)}. \quad (26)$$

The observation space consists of 72 dimensions, with the last 48 representing 16 Lidar measurements of distance to the goal, restricted regions, and obstacles within a 3-meter range. Restricted areas are traversable and less severe constraints to avoid, while obstacles (cubes) are hard constraints that must be strictly avoided, incurring higher costs. The agent must minimize the cumulative cost of violating these constraints over a training episode, as in the following equation (c_t^h and c_t^s are defined in (25c)): $\sum_{t=0}^{T-1} c_t^h + c_t^s$. As such, the optimal policy may not always be able to ensure total avoidance of the obstacles or restricted areas, and must rather minimize this cost. *There are thus three levels of uncertainty arising from randomness/noise in: lidar measurements, robot drift, and randomization of environment entities.* An episode ends after a prescribed maximum number of timesteps (horizon), T (setting a terminal state indicator, d , to 1), during which the robot should visit as many goals as possible.

6.1.1 Training and Evaluation

The agent learns to minimize the stage cost, defined as the change in the goal (denoted as x^g) Euclidean distance between time steps, as in:

$$g_t = -\gamma(\|\mathbf{x}_t^a - \mathbf{x}_t^g\|) - \|\mathbf{x}_{t-1}^a - \mathbf{x}_{t-1}^g\| - c_g,$$

where x_t^g and x_{t-1}^g are the goal distance values at the current and previous time steps, and c_g is a positive scalar. To encourage exploration, we applied an epsilon-greedy linear exploration schedule, i.e., $\max\{t(\epsilon_T - \epsilon_0)\Delta t^{-1}, \epsilon_T\}$. To train all permutations of the QR-AVI (comprising 32 uniformly-distributed quantile fractions), we employed a Feedforward Neural Network with three fully-connected (dense) layers containing two hidden layers (of dimension 120 and 84, respectively) with ReLU activation functions (denoted hereafter as $f_{ac}(\cdot)$), and an output layer that produces values for each (control) input-quantile pair at each time step.

For the KDE cost distribution estimation, we used a Gaussian kernel function with a bandwidth determined by *Scott's rule* [28], i.e., $h = B^{0.2}$, and trained ρ -QR-AVI for $\beta = 0.9$ and 0.95 . On Fig. 3, we plot training curves for the expected cumulative cost Fig. 3a, risk Fig. 3b, and quantile loss

Fig. 3c for all QR-AVI variants. We evaluated the models using five random seeds (0, 5, 10, 15, 20), with 20 episodes per seed, resulting in a total of 100 test episodes. Each seed ensures reproducibility by initializing the random number generator. Next, we computed the average action value, constraint violation cost, number of successful episodes, and goal success rate over all seeds to compare the performance of the algorithms. Here, the success rate represents the number of times the agent reaches the goal, averaged over all 100 test episodes. In the foregoing experiments, we used the training and evaluation hyperparameters listed on Table 2.

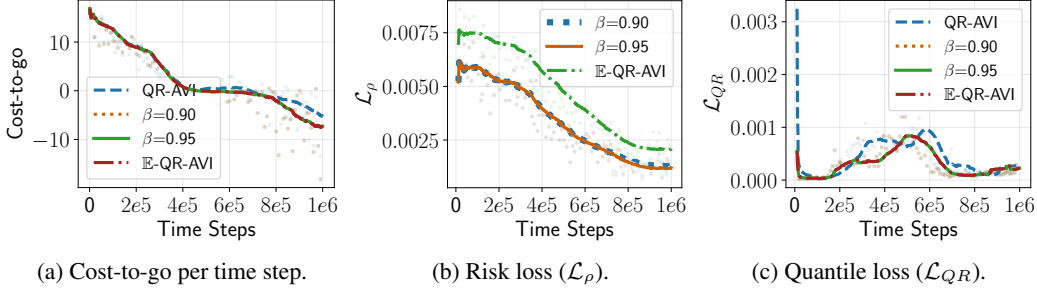


Figure 3: Evolution of the (training) expected cumulative cost, risk loss, and quantile loss for the reach-avoid navigation task.

Table 2: Training and Evaluation Hyperparameters

Param.	Value	Param.	Value	Param.	Value
B, α	128, $2.5e-4$	c_{\max}, β	0.1, $\{.9, .95\}$	γ, N_τ, T	0.99, 32, 1000
$\epsilon_0, \epsilon_T, \kappa$	1.0, 0.05, 1.0	$ \mathcal{D} $	$0.5e6$	Upd. Freq.	10 (train), 500 (target)

6.2 Juxtaposition with the Risk-Neutral Algorithm

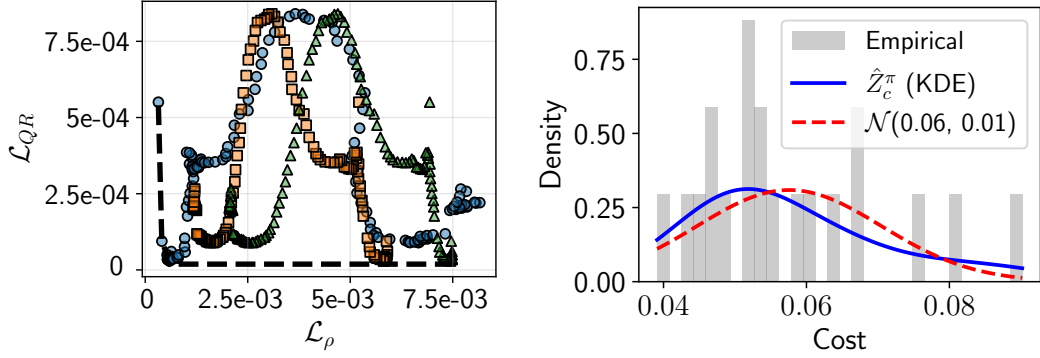
We compare the risk-sensitive QR-AVI against the nominal and expected-value configurations across evaluation metrics. Table 3 juxtaposes our risk-sensitive adaptation with the baselines on the training and evaluation metrics. From the plots, we notice a marked improvement in the average expected cumulative cost for the risk-sensitive QR-AVI than the baseline, with a mostly consistent cost evolution. The agent demonstrates a success rate (that is approximately **37.66%** and **87.45%** higher per episode) than the baselines (nominal and risk-sensitive, respectively). This is reflected in both the increased success rate and the higher total number of successes across all scenarios and episodes.

Table 3: Comparison of success metrics and loss values across different experiments. The reported mean and standard deviation of the average evaluation cost were computed over 100 test episodes. The results obtained using our method are highlighted in gray.

Alg.	Avg. Eval. Cost-to-go	Avg. Eval. Constraint-Violation Cost	Quantile Loss (Avg.)	Total Loss	Total Goals Reached	Normalized Success Rate (%)
QR-AVI	-0.01	0.05 ± 0.01	0.0004	0.0004	239	50%
E-QR-AVI	-0.01	0.06 ± 0.01	0.0003	0.0032	329	75%
ρ -QR-AVI ^{$\beta=0.9$}	-0.01	0.05 ± 0.01	0.0003	0.0023	448	100%
ρ -QR-AVI ^{$\beta=0.95$}	-0.01	0.05 ± 0.01	0.0003	0.0023	448	100%

6.3 Discussions

Here, we expound on the findings presented in the foregoing subsections and highlight a few practical considerations and implementation details.



(a) Pareto front (dashed line) corresponding to data points of the quantile loss (\mathcal{L}_{QR} , y-axis) and risk loss (\mathcal{L}_ρ , x-axis), for the risk-sensitive ($\beta = 0.95$ ●; $\beta = 0.9$ ■) and risk-neutral (▲) cases. (b) Comparing the *tails* of the KDE-estimated cost distribution and a normal distribution with mean 0.06 and standard deviation, 0.1.

Figure 4: Pareto front and cost distribution approximation schemes.

Table 4: β vs. the tail probability difference (Δ_{tail}) between \hat{Z}_c^μ (KDE-based) and $\mathcal{N}(\mu, \sigma^2)$.

β	Δ_{tail}
0.90	0.042
0.95	0.041
0.99	0.027

6.3.1 Training and Evaluation Metrics

Comparing the average quantile losses (Table 3, column 4) reveals that all algorithms achieve near-identical performance, with average losses ranging between $3e-4$ and $4e-4$. The nominal QR-AVI exhibits the highest quantile loss, while the risk-sensitive ($\beta = 0.9$ and $\beta = 0.95$) and expected-value variants achieve slightly lower values of $3e-4$. Comparisons between ρ -QR-AVI and \mathbb{E} -QR-AVI show no significant difference in quantile loss, indicating comparable regression accuracy. Both variants of ρ -QR-AVI also yield similar returns and costs to the baselines but with a substantially higher success rate.

6.3.2 Risk-Performance Trade-offs

Given that we trained the QR-AVI model on a single neural network, a natural question about the performance-risk trade-off arises. Here, performance is quantified by the minimum quantile loss. The Pareto curve, presented in Fig. 4a, depicts the trade-off between the quantile (\mathcal{L}_{QR}) and risk losses (\mathcal{L}_ρ) for the expectation and risk-sensitive configurations of QR-AVI. The plot shows that \mathbb{E} -QR-AVI achieves the lowest quantile loss, indicating better accuracy in predicting cumulative cost, but at the expense of a significantly higher risk loss, highlighting its limitations in risk-sensitive settings. In contrast, the risk-sensitive configurations with $\beta = 0.9$ and $\beta = 0.95$ prioritize safety by achieving lower risk loss values while incurring moderate increases in quantile loss. For safety-critical tasks, the setting with $\beta = 0.95$ is preferable due to its low risk loss, despite a marginally higher quantile loss.

6.3.3 Determining a Fitting Cost Distribution Approximation

Due to environmental randomization, batch costs from the replay buffer may produce empirical distributions with light *right* tails (Fig. 4b) and negligible probability mass for extreme costs. This leads to non-informative upper quantiles coinciding with the mean (see Table 4). To address this, we adopted KDE for a more accurate cost distribution, as simpler methods like softmax or normal distribution ($\mathcal{N}(\mu, \sigma^2)$) often yield uninformative approximations.

7 Conclusion

We introduced a risk-sensitive quantile-based action-value iteration algorithm that balances safety and performance by augmenting the quantile loss with a risk term encoding safety constraints. Our results show that risk sensitivity preserves quantile regression accuracy and ensures consistent performance with tunable risk aversion. The method guarantees convergence to a unique risk-sensitive cost distribution, providing a theoretical foundation. The risk measure is compatible with any off-policy RL model and can be integrated into gradient ascent. Future work will explore dynamic risk parameter adjustments for improved trade-offs in varying conditions.

Acknowledgments

This work was partially supported by the Army Research Laboratory Cooperative Agreement No. W911NF-23-2-0040, a Northrop Grumman Corporation grant, and by the Lockheed Martin Chair in Systems Engineering.

References

- [1] A. Pan, K. Bhatia, and J. Steinhardt. The Effects of Reward Misspecification: Mapping and Mitigating Misaligned Models. *arXiv preprint arXiv:2201.03544*, 2022.
- [2] D. K. Beyer, D. A. Dulo, G. A. Townsley, and S. S. Wu. Risk, Product Liability Trends, Triggers, and Insurance in Commercial Aerial Robots. In *We Robot Conference on Legal & Policy Issues Relating to Robotics. University of Miami School of Law*, volume 4, 2014.
- [3] V. Mnih, K. Kavukcuoglu, D. Silver, A. Graves, I. Antonoglou, D. Wierstra, and M. Riedmiller. Playing Atari with Deep Reinforcement Learning, 2013.
- [4] H. Van Hasselt, A. Guez, and D. Silver. Deep Reinforcement Learning with Double Q-Learning. In *Proceedings of the AAAI Conference on Artificial Intelligence*, volume 30, 2016.
- [5] Z. Wang, T. Schaul, M. Hessel, H. v. Hasselt, M. Lanctot, and N. d. Freitas. Dueling Network Architectures for Deep Reinforcement Learning, 2016.
- [6] A. Kuznetsov, P. Shvechikov, A. Grishin, and D. Vetrov. Controlling Overestimation Bias with Truncated Mixture of Continuous Distributional Quantile Critics, 2020.
- [7] W. Dabney, M. Rowland, M. G. Bellemare, and R. Munos. Distributional Reinforcement Learning with Quantile Regression. *arXiv preprint arXiv:1710.10044*, Oct. 2017.
- [8] G. N. Tasse, T. Love, M. Nemecek, S. James, and B. Rosman. ROSARL: Reward-Only Safe Reinforcement Learning, 2023.
- [9] G. Thomas, Y. Luo, and T. Ma. Safe Reinforcement Learning by Imagining the Near Future. *NeurIPS*, 34:13859–13869, 2021.
- [10] N. P. Farazi, B. Zou, T. Ahamed, and L. Barua. Deep reinforcement learning in transportation research: A review. *Transportation research interdisciplinary perspectives*, 11:100425, 2021.
- [11] J. Ji, B. Zhang, J. Zhou, X. Pan, W. Huang, R. Sun, Y. Geng, Y. Zhong, J. Dai, and Y. Yang. Safety Gymnasium: A Unified Safe Reinforcement Learning Benchmark. *NeurIPS*, 36, 2023.
- [12] R. Fakoor, P. Chaudhari, and A. J. Smola. P3O: Policy-on Policy-off Policy Optimization. In *Proceedings of The 35th Uncertainty in Artificial Intelligence Conference*, pages 1017–1027. PMLR, 2020. URL <https://proceedings.mlr.press/v115/fakoor20a.html>.
- [13] C. Ying, X. Zhou, H. Su, D. Yan, N. Chen, and J. Zhu. Towards Safe Reinforcement Learning via Constraining Conditional Value-at-Risk, Sept. 2022.
- [14] D. P. Bertsekas. Model predictive control and reinforcement learning: A unified framework based on dynamic programming, 2024. URL <http://arxiv.org/abs/2406.00592>.

- [15] P. Artzner, F. Delbaen, J.-M. Eber, and D. Heath. Coherent Measures of Risk. *Mathematical Finance*, 9(3):203–228, 1999. ISSN 1467-9965. doi:10.1111/1467-9965.00068.
- [16] D. Nass, B. Belousov, and J. Peters. Entropic Risk Measure in Policy Search. In *IROS*, pages 1101–1106. IEEE, 2019.
- [17] R. T. Rockafellar. Risk and Utility in the Duality Framework of Convex Analysis. *From Analysis to Visualization: A Celebration of the Life and Legacy of Jonathan M. Borwein, Callaghan, Australia, September 2017*, pages 21–42, 2020.
- [18] C. Mavridis, E. Noorani, and J. S. Baras. Risk Sensitivity and Entropy Regularization in Prototype-Based Learning. In *2022 30th Mediterranean Conference on Control and Automation (MED)*, pages 194–199. IEEE, 2022.
- [19] E. Noorani and J. S. Baras. Risk-Sensitive Reinforcement Learning: A Monte Carlo Policy Gradient Algorithm for Exponential Performance Criteria. In *CDC*. IEEE, 2021.
- [20] E. Noorani and J. S. Baras. Risk-Sensitive Reinforcement Learning and Robust Learning for Control. In *CDC*. IEEE, 2021.
- [21] E. Noorani, C. Mavridis, and J. Baras. Risk-Sensitive Reinforcement Learning with Exponential Criteria. *arXiv preprint arXiv:2212.09010*, 2022.
- [22] Y. Chow, M. Ghavamzadeh, L. Janson, and M. Pavone. Risk-Constrained Reinforcement Learning with Percentile Risk Criteria, Apr. 2017.
- [23] B. W. Silverman. *Density Estimation for Statistics and Data Analysis*. Routledge, 2017. ISBN 978-1-315-14091-9. doi:10.1201/9781315140919.
- [24] E. Hüllermeier and W. Waegeman. Aleatoric and Epistemic Uncertainty in Machine Learning: An Introduction to Concepts and Methods. *Machine Learning*, 110(3):457–506, Mar. 2021. ISSN 1573-0565. doi:10.1007/s10994-021-05946-3.
- [25] Y.-C. Chen. A Tutorial on Kernel Density Estimation and Recent Advances. *Biostatistics & Epidemiology*, 2017. ISSN 2470-9360.
- [26] S. H. Lim and I. Malik. Distributional reinforcement learning for risk-sensitive policies. *Advances in Neural Information Processing Systems*, 35:30977–30989, 2022. URL https://papers.nips.cc/paper_files/paper/2022/hash/c88a2bd0e793550d0e885aa6e31ca277-Abstract-Conference.html.
- [27] A. T. Bharucha-Reid. Fixed Point Theorems in Probabilistic Analysis. *Bulletin of the American Mathematical Society*, 82(5):641–657, 1976. ISSN 0002-9904, 1936-881X. doi:10.1090/S0002-9904-1976-14091-8.
- [28] D. W. Scott and G. R. Terrell. Biased and Unbiased Cross-Validation in Density Estimation. *Journal of the American Statistical Association*, 82(400):1131–1146, 1987. ISSN 0162-1459. doi:10.2307/2289391.